Distributed Secondary Control Based on Dynamic Diffusion Algorithm for Current Sharing and Average Voltage Regulation in DC Microgrids

Dawei Liao, Fei Gao, *Member*, *IEEE*, Daniel J. Rogers, *Senior Member*, *IEEE*, Wentao Huang, *Member*, *IEEE*, Dong Liu, *Senior Member*, *IEEE*, and Houjun Tang

***Abstract*—This paper introduces a distributed secondary control scheme for achieving current sharing and average voltage regulation objectives in a DC microgrid. The proposed scheme employs a dynamic diffusion algorithm (DDA) instead of the consensus algorithm to enable distributed communication among converters. To help understand DDA, the relation of DDA and other diffusion algorithms is discussed in detail and its superiority is shown by comparison with diffusion and consensus algorithms. Furthermore, considering the discrete nature and different sampling time of the digital controller and communication network, a *z*-domain model of the entire DC microgrid is established. The influence of communication and secondary control parameters on the system stability is investigated. Based on the established model, the tolerable communication rates are obtained. Real-time simulations conducted on the OPAL-RT platform validate the effectiveness of the proposed scheme, showcasing its advantages in terms of convergence speed and stability.**

***Index Terms*—Cooperative control, DC microgrid, diffusion algorithm, discrete-time modeling, distributed secondary control.**

I. Introduction

MICROGRID (MG) provides a convenient and efficient interface to distributed energy resources (DERs), energy storage systems (ESSs), and loads [1]. Compared with AC MGs, because of the absence of frequency regulation, synchronization and reactive power management, DC MGs achieve higher efficiency with fewer conversion stages when faced with DC loads and ESSs. Considering these advantages, DC MGs are prevalently adopted in terrestrial applications and marine/aircraft onboard electrical systems [2], [3].

A hierarchical control structure with three control layers is widely utilized in DC MGs [4], [5]. The primary control layer deals with local voltage/current regulation and power/current sharing. Within the primary control layer, droop control, a decentralized method that exclusively relies on local information and necessitates no communication links, is frequently employed to ensure proper load sharing among converters. On the other hand, the secondary control layer focuses on addressing voltage deviation caused by droop control and refining power sharing precision. This paper centers its attention on the primary and secondary control layers.

Secondary control strategies can be classified into centralized, distributed, and decentralized control strategies based on the communication means among converters [6]. In centralized control, a central controller is mandatory to collect global information and send commands to all converters. However, centralized control is susceptible to single points of failure (SPOFs). On the contrary, decentralized control is less complicated to deploy but may not deliver accurate load allocation or achieve MG global optimization [7]. As a result, distributed secondary control has been widely adopted in recent years. This strategy necessitates less communication investment since it only requires a sparse network to communicate among neighboring converters [8]. Additionally, it is impervious to communication breakdowns since there is no central controller [9].

Previous researches have tried implementing distributed control with various approaches [10] - [13]. Reference [11] achieves state of charge (SOC) balancing through DC bus signaling and a secondary controller for balancing. In [12], a hybrid method with both voltage-shifting and slope-adjusting approaches is proposed, which equalizes not only output currents but also output impedances of converters. Reference [13] proposes a current regulator that calculates the weighted average currents of all converters and a voltage regulator that shifts the droop curve to reach the accurate current sharing and suitable voltage regulation.

In recent years, secondary control strategies utilizing consensus algorithms have garnered significant attention and have been widely investigated. Several research studies have explored optimal design for communication networks [14], stability analysis taking into account communication delays [15], event-triggered mechanisms [16], distributed sliding

Manuscript received: October 12, 2022; revised: March 21, 2023; accepted: June 24, 2023. Date of CrossCheck: June 24, 2023. Date of online publication: August 29, 2023.

This work was supported by the Natural Science Foundation of Shanghai (No. 22ZR1429800) and China Southern Power Grid Company Limited (No. GDKJXM20222178).

D. Liao, F. Gao (corresponding author), W. Huang, D. Liu, and H. Tang are with the Department of Electrical Engineering, Shanghai Jiao Tong University, Shanghai, China (e-mail: alonekayak@sjtu.edu.cn; fei.gao@sjtu.edu.cn; hwt8989@sjtu.edu.cn; dongliu@sjtu.edu.cn; hjtang@sjtu.edu.cn).

D. J. Rogers is with the Department of Engineering Science, University of Oxford, Oxford OX1 2JD, U.K. (e-mail: dan.rogers@eng.ox.ac.uk).

DOI: 10.35833/MPCE.2022.000668

mode controllers [17], and passivity-based controllers [18]. Additionally, various variants of consensus algorithms, such as proportional-integral (PI) consensus and ratio consensus, have been developed and implemented in secondary control [19]-[21]. While some studies have proposed fixed-time or finite-time structures to improve the convergence speed of the system [22]-[25], most of the related works still employ consensus algorithms.

Compared with consensus algorithm, diffusion algorithm is a superior solution to distributed estimation and adaptation problems [26]. Diffusion networks have faster convergence speed and reach lower mean-square deviation than consensus networks. However, its application in MGs is limited. In [27]-[29], the diffusion algorithm is applied in tertiary control layer to achieve optimal operation of an MG. Reference [30] applies an exact diffusion algorithm (EDA) in the tertiary control in MGs to achieve economic dispatch.

Besides tertiary control, the secondary control based on diffusion is also rarely studied. Reference [31] proposes a secondary control scheme based on the diffusion algorithm to achieve reactive power sharing and voltage control of an offshore wind farm. But the system stability is not analyzed. Reference [32] implements a secondary controller using a diffusion algorithm in an AC MG, of which the stability is analyzed via a continuous-time small-signal model. Reference [33] proposes a dynamic diffusion algorithm (DDA) based secondary control scheme in a single-bus DC MG, which requires the estimation of line impedances. In addition, the relation among different diffusion algorithms is not revealed in the aforementioned studies.

Additionally, there has been limited research on discrete-time (DT) secondary control schemes, which are more practical than continuous-time ones. For instance, [34] develops a DT event-triggered secondary control scheme and proves its asymptotic convergence using Lyapunov synthesis. In [35], a DT secondary controller with a voltage observer using only the local current sharing errors is proposed. Although the upper bounds of control gains and constant power loads (CPLs) are obtained, the constraints on sampling periods are not quantitatively analyzed. In [36], a DT secondary control scheme based on the scheme in [37] is introduced. However, the upper bound of communication intervals is dependent on sampling values, and the dynamics of the inner control loops are neglected in the above studies. As the secondary control bandwidths increase rapidly due to the development of communication technology, the impact of the inner control loops becomes more significant.

To fill the aforementioned gaps, this paper proposes a distributed secondary control scheme using DDA in a multiple-bus DC MG, of which the stability is analyzed in DT domain. The main contributions of this paper can be highlighted as follows.

1) The relation between DDA and other diffusion algorithms is fully demonstrated and the advantages of DDA is clearly shown.

2) A distributed secondary control scheme based on DDA is designed to achieve average voltage regulation and proportional current sharing in a multiple-bus DC MG without knowledge of feeder line parameters. Convergence speed of the system is improved compared with finite-time controllers.

3) A detailed DT z-domain model of the whole system considering different sampling time of digital controllers and communication network is established, based on which the tolerable communication rate of the proposed scheme is obtained and is further validated via real-time simulations.

The rest of this paper is organized as follows. Section II shows the derivation of DDA and its superiority to traditional consensus and diffusion algorithms. Section III presents the proposed distributed secondary control scheme based on DDA. In Section IV, an overall DT model is described, based on which the stability analysis of overall system is conducted considering secondary control parameters and communication rate. Section V presents the real-time simulation results. Finally, Section VI concludes this paper.

II. Derivation of DDA and Its Superiority to Traditional Consensus and Diffusion Algorithms

A diffusion algorithm was originally proposed for adaptive networks which consist of a collection of agents to solve an optimization problem in a distributed fashion [38]. In previous studies, the diffusion and its variants, EDA and DDA, are adopted in tertiary and secondary control layers [30], [33]. But the relation between them has not been mentioned yet. In order to better introduce DDA, this section shows the derivation of DDA as well as its superior performance over traditional consensus and diffusion algorithms.

A. Preliminaries on Graph Theory

The communication network among converters is denoted as a graph $\mathcal{G}=(\mathcal{V},\mathcal{E},\boldsymbol{A})$, where $\mathcal{V}$ denotes the set of nodes, $\mathcal{E}\supseteq\mathcal{V}\times\mathcal{V}$ denotes the set of edges between two nodes, and $\boldsymbol{A}\in\mathbb{R}^{n\times n}$ denotes the adjacency matrix. Each node in the set $\mathcal{V}=\{1,2,\ldots,n\}$ represents a distributed secondary controller and edges in the set $\mathcal{E}$ represent the communication links among controllers. If there is a link between node i and node j, the two nodes are adjacent. Entities of the adjacency matrix $\boldsymbol{A}$ are denoted as a_{ij}, which is defined by specific rules and network topology. If node i and node j are adjacent, $a_{ij}>0$, and otherwise $a_{ij}=0$. The set of neighboring nodes of node i is defined as $\mathcal{N}_i=\left\{j\in\mathcal{V}\,\middle|\,(i,j)\in\mathcal{E}\right\}$.

B. Derivation of DDA

In the following derivation, an aggregated optimization problem of the form is considered:

$$\omega^*=\arg\min_{\omega\in\mathbb{R}}J(\omega)=\arg\min_{\omega\in\mathbb{R}}\sum_{i=1}^{n}J_i(\omega) \tag{1}$$

where $J_i(\omega)$ is the cost function of agent i, which is differentiable and convex; n is the number of agents; and ω is the decision variable. All agents seek to achieve the optimal solution ω^* only through communication with their neighbors.

To solve this problem, a diffusion algorithm is proposed in [39], which typically has an adapt-then-combine (ATC) structure as shown in (2).

$$\begin{cases} \psi_i(k) = \omega_i(k-1) - \mu \nabla J_i\big(\omega_i(k-1)\big) \\ \omega_i(k) = \sum\limits_{j \in \mathcal{N}_i} a_{ij} \psi_j(k) \end{cases} \tag{2}$$

where $\omega_i(k)$ is the state of node i at sample k; $\psi_i(k)$ is the intermediate variable for node i at sample k; and μ is the coefficient of positive step size. Reference [26] has already shown that diffusion algorithm has a wider range of step sizes ensuring stability and a smaller spectral radius than consensus algorithms, which means that diffusion networks converge faster than consensus networks.

Nevertheless, this diffusion can be interpreted as the diagonally-weighted incremental iteration to solve the approximate penalized form of the original problem (1) [40]. When the step size is constant, the iteration in (2) converges towards a neighborhood of square-error size $O(\mu^2)$ around the optimal solution ω^*. Therefore, there always exists a bias between its solution and the real solution ω^*.

To remove the bias, a correction step is introduced into (2), and thus EDA proposed in [40] can be obtained as:

$$\begin{cases} \psi_i(k) = \omega_i(k-1) - \mu \nabla J_i\big(\omega_i(k-1)\big) \\ \phi_i(k) = \psi_i(k) + \omega_i(k-1) - \psi_i(k-1) \\ \omega_i(k) = \sum\limits_{j \in \mathcal{N}_i} \bar{a}_{ij} \phi_j(k) \end{cases} \tag{3}$$

where $\phi_i(k)$ is the newly introduced intermediate variable; and $\bar{a}_{ij}$ is the entity of the matrix $\bar{\boldsymbol{A}} = \big(\boldsymbol{A} + \boldsymbol{I}_n\big)/2$, and $\boldsymbol{I}_n$ is the identity matrix.

In the secondary control, distributed algorithms are utilized in each controller to track a global average of a sampled value, such as output current and voltage. One way to achieve real-time tracking of the average of samples $\{r_i(k)\}$ is to consider the following cost function for each agent i:

$$J_i\big(\omega(k)\big) = \frac{1}{2}\big(\omega - r_i(k)\big)^2 \tag{4}$$

The corresponding aggregated cost function is expressed as:

$$J\big(\omega(k)\big) = \frac{1}{2}\sum_{i=1}^{n}\big(\omega - r_i(k)\big)^2 \tag{5}$$

The optimal solution of (5) will be exactly the average of the samples:

$$\omega^* = \frac{1}{n}\sum_{i=1}^{n} r_i(k) \tag{6}$$

Thus, by substituting (4) into (3), a variant of diffusion to track the average of samples, DDA, is obtained as [41]:

$$\begin{cases} \psi_i(k) = (1-\mu)\omega_i(k-1) + \mu r_i(k) \\ \phi_i(k) = \psi_i(k) + \omega_i(k-1) - \psi_i(k-1) \\ \omega_i(k) = \sum\limits_{j \in \mathcal{N}_i} \bar{a}_{ij} \phi_j(k) \end{cases} \tag{7}$$

To guarantee stable convergence of the algorithm, the step size μ and the adjacency matrix $\boldsymbol{A}$ should satisfy certain conditions. The optimal choice of step size has not been reported by any research yet, but usually the step size should be limited within (0, 2], as discussed in Section IV.

$\boldsymbol{A}$ must be a right stochastic matrix, which means $\boldsymbol{A}\cdot\mathbf{1} = \mathbf{1}$ [40]. In addition, the network graph should be strongly connected, which means that there exists at least one path between any two nodes and at least one diagonal entry of $\boldsymbol{A}$ is non-zero. For the convenience of comparison, following the rules in [33] and [42], Metropolis rule [26] is adopted in this paper:

$$a_{ij} = \begin{cases} \dfrac{1}{\max\{n_i, n_j\}} & j \in \mathcal{N}_i, i \neq j \\ 1 - \sum\limits_{j \in \mathcal{N}_i} a_{ij} & i = j \\ 0 & j \notin \mathcal{N}_i \end{cases} \tag{8}$$

where n_i is the number of neighbors of node i.

C. Comparison Between Consensus and Diffusion Algorithms

Consensus algorithm is commonly used to address distributed estimation problems in secondary control layer of MG. Thus, in this subsection, first, a dynamic consensus algorithm (DCA) with an optimal step size as described in [42] is used for comparison.

A six-node communication network with different topologies is tested to verify the convergence of DDA. The results of DDA are compared with those of DCA. Sampled values of each node r_1-r_6 as well as communication rate of the network T_{com} are shown in Table I. The convergence of the network under different topologies is shown in Fig. 1.

TABLE I
SAMPLED VALUES OF EACH NODE AND COMMUNICATION RATE OF A SIX-NODE COMMUNICATION NETWORK

Parameter	Value	Parameter	Value
r_1	1	r_5	20
r_2	7	r_6	25
r_3	13	T_{com}	10 ms
r_4	18		

As shown in Fig. 1, both DDA and DCA can converge under all four topologies. Among the four topologies, cross topology brings the fastest convergence speed and line topology shows the slowest convergence speed. Compared with the results of DCA, DDA has nearly the same performance under line topology and shows faster convergence speed under star, ring, and cross topologies.

Additionally, the convergence performance of DDA is compared with that of traditional diffusion algorithm. The mean square error (MSE) is defined below to quantify the convergence performance:

$$MSE = \frac{1}{n}\sum_{i=1}^{n}\big(\omega_i - r_i\big)^2 \tag{9}$$

Equation (9) represents the convergence accuracy at the steady state. A lower MSE implies a more accurate convergence. The MSEs of traditional diffusion algorithm and DDA under a step size of 0.1 after 10000 iterations are compared in Table II. It is observed that DDA can reach a much lower MSE than traditional diffusion algorithms.

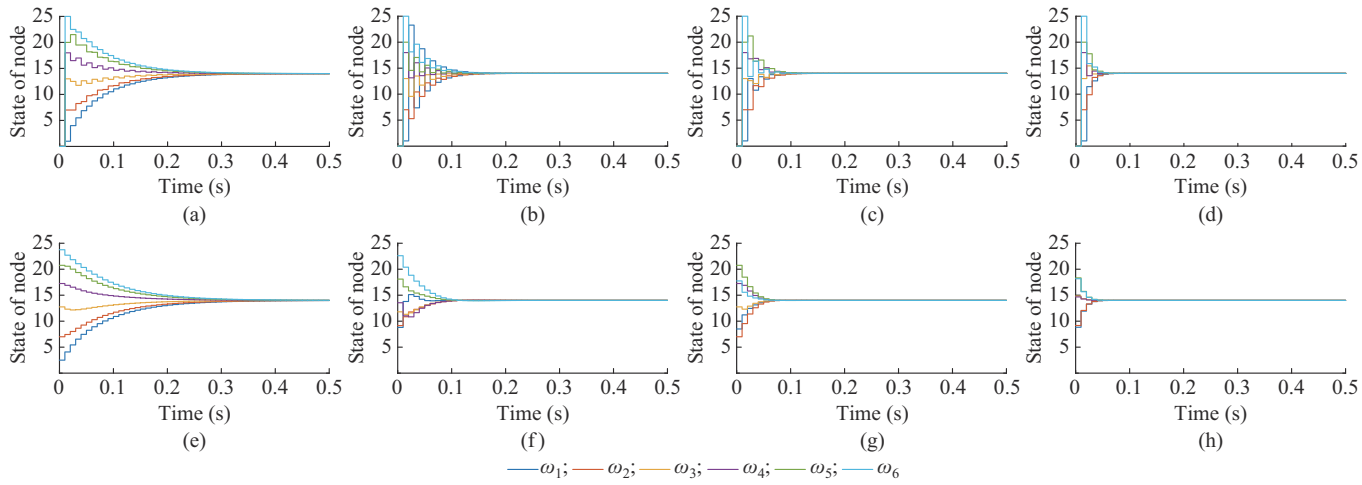

Fig. 1. Convergence of a six-node communication network under different topologies using DCA and DDA. (a) DCA under line topology. (b) DCA under star topology. (c) DCA under ring topology. (d) DCA under cross topology. (e) DDA under line topology. (f) DDA under star topology. (g) DDA under ring topology. (h) DDA under cross topology.

TABLE II
MSE OF TRADITIONAL DIFFUSION ALGORITHM AND DDA

Algorithm	MSE			
	Line topology	Ring topology	Cross topology	Full topology
Diffusion	1.394×10^{0}	2.742×10^{-2}	1.077×10^{-3}	1.093×10^{-3}
DDA	5.762×10^{-27}	3.029×10^{-28}	1.396×10^{-20}	2.346×10^{-24}

III. PROPOSED DISTRIBUTED SECONDARY CONTROL BASED ON DDA

Figure 2 shows the DC MG with multiple buses under study. Distributed generators (DGs) are connected to local buses through LC filters, delivering power to loads that locate at different DC buses. Each converter is equipped with a hierarchical controller that contains two layers: distributed secondary control and local primary control. While the local primary control regulates output voltage and current, the distributed secondary control communicates with neighbors through communication links and sends a correction signal to the local primary control layer to achieve cooperative control among converters. It is worth noting that the communication network does not need to have the same topology as the electrical network.

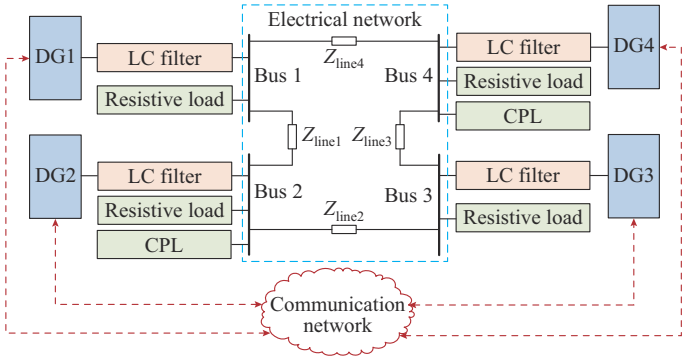

Fig. 2. Layout of a DC MG with multiple buses.

A. Local Primary Control Based on Droop Control

The local primary control layer incorporates three cascaded control parts, which are droop control, primary voltage PI control, and primary current PI control. In this control layer, only local measurements are required. In the droop control, as shown in Fig. 3, a virtual output resistance R_{di} is introduced:

$$v_{\mathrm{ref},i}^{\mathrm{droop}} = V^{*} - R_{\mathrm{d}i} i_{L,i} \tag{10}$$

where $v_{\mathrm{ref},i}^{\mathrm{droop}}$ is the reference voltage given by droop control; V^{*} is the nominal bus voltage; and $i_{L,i}$ is the inductor current of converter i.

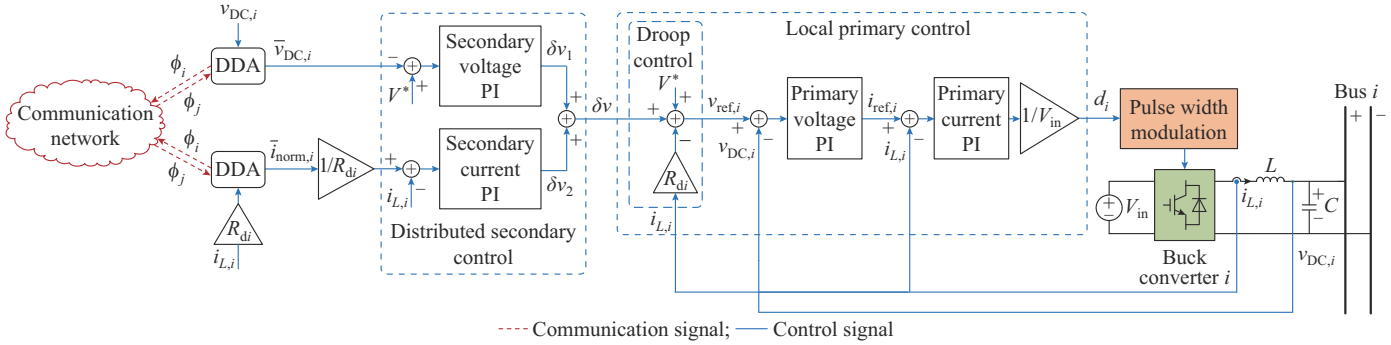

Fig. 3. Proposed distributed secondary control scheme.

If the primary voltage PI control and current PI control are properly designed, the bus voltage can track the reference given by the droop control:

$$v_{\mathrm{DC},i}=v_{\mathrm{ref},i}^{\mathrm{droop}} \tag{11}$$

where $v_{\mathrm{DC},i}$ is the bus voltage of DG i. Thus, bus voltages deviate from the nominal value V^* with only the local primary control based on droop control applied.

Moreover, the current sharing performance is dependent on the electrical network besides virtual resistances. At steady state, the output currents of converters are equal to inductor currents:

$$i_{\mathrm{DC},i}=i_{L,i} \tag{12}$$

where $i_{\mathrm{DC},i}$ is the output current of converter i, which is also the current injection to bus i. Considering (10)-(12), due to the line impedances between buses, bus voltages differ from each other, resulting in unequal current sharing.

Therefore, to address the voltage deviation and current sharing problems, the droop curve is shifted by a correction term δv:

$$v_{\mathrm{ref},i}=V^*-R_{\mathrm{d}i}i_{L,i}+\delta v \tag{13}$$

where $v_{\mathrm{ref},i}$ is the reference voltage given by droop control and secondary control.

The cascaded inner control loops are expressed as:

$$i_{\mathrm{ref},i}=G_{\mathrm{V}}(s)\left(v_{\mathrm{ref},i}-v_{\mathrm{DC},i}\right) \tag{14}$$

$$d_i=\frac{1}{V_{\mathrm{in}}}G_{\mathrm{C}}(s)\left(i_{\mathrm{ref},i}-i_{L,i}\right) \tag{15}$$

where $i_{\mathrm{ref},i}$ is the reference current; d_i is the duty cycle; V_{in} is the input voltage of the converter; and $G_{\mathrm{V}}(s)$ and $G_{\mathrm{C}}(s)$ represent the primary voltage PI control and current PI control, respectively.

B. Proposed Distributed Secondary Control

Secondary control aims to eliminate the voltage deviation and improve the current sharing accuracy. First, the average voltage of all buses is supposed to be the nominal voltage V^*:

$$\frac{1}{n}\sum_{i=1}^{n}v_{\mathrm{DC},i}=V^* \tag{16}$$

Second, the currents should be allocated according to the droop gains (17), which is equivalent to (18).

$$\frac{i_{L,i}}{i_{L,j}}=\frac{R_{\mathrm{d}j}}{R_{\mathrm{d}i}} \tag{17}$$

$$i_{\mathrm{norm},i}=R_{\mathrm{d}i}i_{L,i}=R_{\mathrm{d}j}i_{L,j}=i_{\mathrm{norm},j} \tag{18}$$

where $i_{\mathrm{norm},i}$ is the normalized current.

The proposed distributed secondary control scheme is shown in Fig. 3. Two aforementioned objectives are achieved by the secondary voltage PI control and secondary current PI control, respectively, which generate two correction terms, δv_1 and δv_2:

$$\delta v_1=\left(K_{\mathrm{psv}}+\frac{K_{\mathrm{isv}}}{s}\right)\left(V^*-\bar{v}_{\mathrm{DC},i}\right) \tag{19}$$

$$\delta v_2=\left(K_{\mathrm{psc}}+\frac{K_{\mathrm{isc}}}{s}\right)\left(\frac{\bar{i}_{\mathrm{norm},i}}{R_{\mathrm{d}i}}-i_{L,i}\right) \tag{20}$$

where K_{psv} and K_{isv} are the proportional and integral gains for the secondary voltage PI control, respectively; K_{psc} and K_{isc} are the proportional and integral gains for the secondary current PI control, respectively; $\bar{v}_{\mathrm{DC},i}$ is the average bus voltage estimated locally at converter i; and $\bar{i}_{\mathrm{norm},i}$ is the average normalized current estimated locally at converter i. The two terms are combined to shift the droop curve:

$$\delta v=\delta v_1+\delta v_2 \tag{21}$$

The references for the secondary voltage PI control and secondary current PI control include $\bar{v}_{\mathrm{DC},i}$ and $\bar{i}_{\mathrm{norm},i}$. In the proposed scheme, secondary controllers estimate the average values through a sparse communication network using DDA. For average voltage estimation, the observation variable $r_i(k)$ in DDA is replaced by the locally measured output voltage $v_{\mathrm{DC},i}$ and the state variable $\omega_i(k)$ is the locally estimated average voltage $\bar{v}_{\mathrm{DC},i}$. For average normalized current estimation, the observation variable $r_i(k)$ in DDA is the local normalized current $i_{\mathrm{norm},i}$ and the state variable $\omega_i(k)$ is the locally estimated average normalized current $\bar{i}_{\mathrm{norm},i}$.

Remark 1: according to (13) and (21), if the local primary control can well follow the reference voltage, the average voltage can be expressed as:

$$\begin{aligned}\bar{v}=&\frac{1}{n}\sum_{i=1}^{n}\left(V^*-R_{\mathrm{d}i}i_{L,i}+\delta v_{1,i}+\delta v_{2,i}\right)=\\&\frac{1}{n}\sum_{i=1}^{n}V^*+\frac{1}{n}\sum_{i=1}^{n}\left(-R_{\mathrm{d}i}i_{L,i}+\delta v_{1,i}\right)+\frac{1}{n}\sum_{i=1}^{n}\delta v_{2,i}\end{aligned} \tag{22}$$

When the gains in the secondary current PI control are the same, the sum of $\delta v_{2,i}$ satisfies:

$$\sum_{i=1}^{n}\delta v_{2,i}=\left(K_{\mathrm{psc}}+\frac{K_{\mathrm{isc}}}{s}\right)\sum_{i=1}^{n}\left(\frac{\bar{i}_{\mathrm{norm},i}}{R_{\mathrm{d}i}}-i_{L,i}\right)=0 \tag{23}$$

Thus, the outputs of secondary current PI control impose no effect on the average voltage. Therefore, while determining the secondary control gains, K_{psv} and K_{isv} in secondary voltage PI control can be considered first regardless of secondary current PI control. After a desired response of average voltage restoration is achieved, secondary current PI control gains can be designed to improve current sharing performance.

Remark 2: when designing a traditional dual-loop controller or other local cascaded controllers, one of the important considerations is that upper controllers should be decoupled from the lower controllers. In distributed secondary control, control parameters should also be designed according to the communication conditions, which will be further illustrated in Section IV.

IV. Stability Analysis

In this section, a DT z-domain model of the MG is established, based on which the system stability is investigated under different control parameters. Moreover, the tolerable communication rate based on DDA is compared with that of DCA. The specifications of the MG as well as parameters of loads and tie-lines are listed in Tables III and IV. $R_{\mathrm{line}i}$, $L_{\mathrm{line}i}$,

$R_{\text{load}i}$, and $P_{\text{CPL}i}$ $(i=1,2,3,4)$ are the line resistances, line inductances, load resistances, and power of constant power loads, respectively. The communication network is of ring topology.

TABLE III
ELECTRICAL AND CONTROL PARAMETERS OF MG

Category	Parameter	Value
Input voltage	V_{in}	100 V
LC filter	L	1.8 mH
	C	2200 μF
Droop gain	R_{di}	0.1
Primary voltage PI	K_{pv}	13
	K_{iv}	800
Primary current PI	K_{pc}	5
	K_{ic}	100
Secondary voltage PI	K_{psv}	0.02
	K_{isv}	23
Secondary current PI	K_{psc}	0.1
	K_{isc}	5.5
Controller sampling time	T_{d}	100 μs
Communication rate of network	T_{com}	10 ms
Step size	μ	0.5

TABLE IV
PARAMETERS OF LOADS AND TIE-LINES

Parameter	Value
R_{line1}, R_{line2}, R_{line3}, R_{line4}	0.1, 0.12, 0.1, 0.13 Ω
L_{line1}, L_{line2}, L_{line3}, L_{line4}	0.011, 0.013, 0.011, 0.016 mH
R_{load1}, R_{load2}, R_{load3}, R_{load4}	13, 9, 8, 7 Ω
P_{CPL1}, P_{CPL2}, P_{CPL3}, P_{CPL4}	0, 300, 0, 300 W

A. DT System Modeling

The modeling method in [42] is employed in order to consider the DT feature of communication networks and different sampling time of electrical networks, digital controllers, and communication networks. These three parts of the system, i. e., the electrical network, the digital controllers, and the communication network, are modeled separately first and then discretized, resampled, and integrated into an overall model. The overall model encompasses a z-domain communication network model with a sampling time of T_{com}, a z-domain controller model with a sampling time of T_{d}, and an s-domain main circuit model. The integration process of the overall model is depicted in Fig. 4 in detail. $\boldsymbol{d}$, $\boldsymbol{v}_{\text{DC}}$, $\boldsymbol{i}_L$, $\bar{\boldsymbol{v}}_{\text{DC}}$, $\bar{\boldsymbol{i}}_{\text{norm}}$ are the vector variables of duty cycles, output voltages, inductor currents, normalized output voltages, and normalized currents, respectively; G_{MG}, G_{CTRL}, and G_{COM} are the transfer functions of the electrical network model, the digital controller, and the communication network, respectively; G_{MGCT} is the transfer function of the combined model of the electrical network and the digital controller; and G_{ALL} is the transfer function of the overall model.

Step 1: the continuous-time main circuit model is discretized using zero-order-hold (ZOH) method with a sampling time of T_{d}.

Step 2: the DT controller model and main circuit model are combined by connecting the corresponding input/output ports.

Step 3: the model is resampled with a sampling time T_{com}.

Step 4: by connecting the corresponding input/output ports, the model in *Step 3* is combined with the communication network model to obtain the overall model.

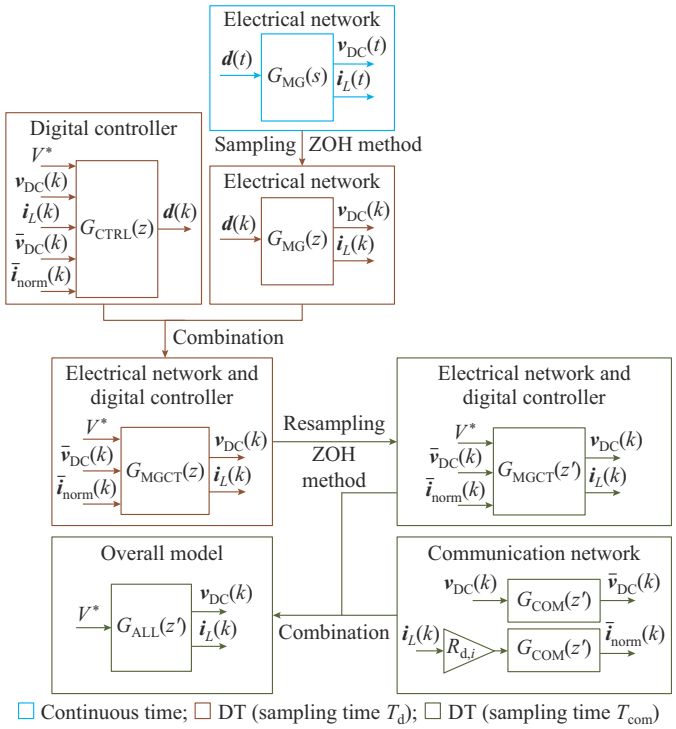

Fig. 4. Integration process of overall model containing electrical network, digital controllers, and communication network.

B. Observation Weight μ

The observation weight μ in DDA is an important parameter that affects system stability. The root contour of the overall model with μ changing from 0.5 to 2.1 with a step of 0.2 is shown in Fig. 5. T is the sampling period. The blue stars represent the poles of the system. The arrows show the changing direction of poles as the parameter changes. It can be observed that when the observation weight is between 0.5 and 1.9, the system stability is guaranteed.

C. Integral Gain of Secondary Voltage Controller K_{isv}

Secondary PI controllers also affect the cooperated control among converters. The root contour with the integral gain of secondary voltage PI controller K_{isv} changing from 50 to 750 with a step of 25 is shown in Fig. 6. The upper bound of K_{isv} ensuring the system stabilty is 700.

D. Communication Rate T_{com}

Communication rate T_{com} also influences the stability of cooperative strategies [43]. The root contour with communication rate changing from 30 to 300 ms with a step of 30 ms is shown in Fig. 7. The upper bound of communication rate is 300 ms according to the root contour, indicating that an increasing T_{com} deteriorates the communication conditions among converters and finally results in instability.

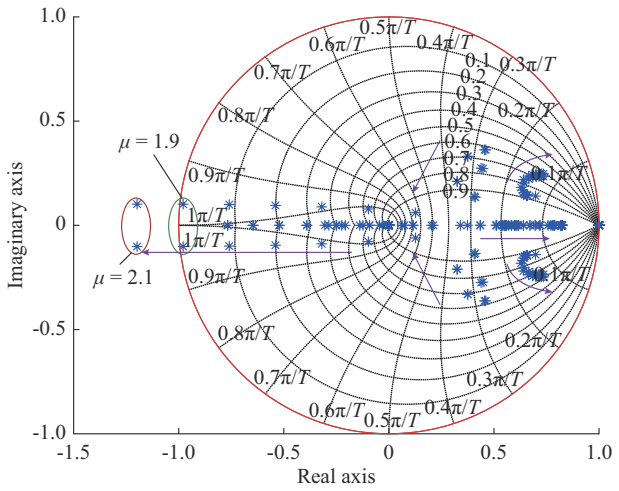

Fig. 5. Root contour with μ changing from 0.5 to 2.1 with a step of 0.2.

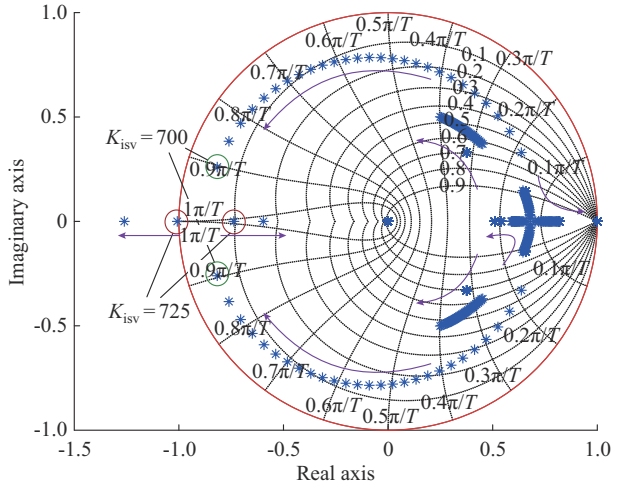

Fig. 6. Root contour with K_{isv} changing from 50 to 750 with a step of 25.

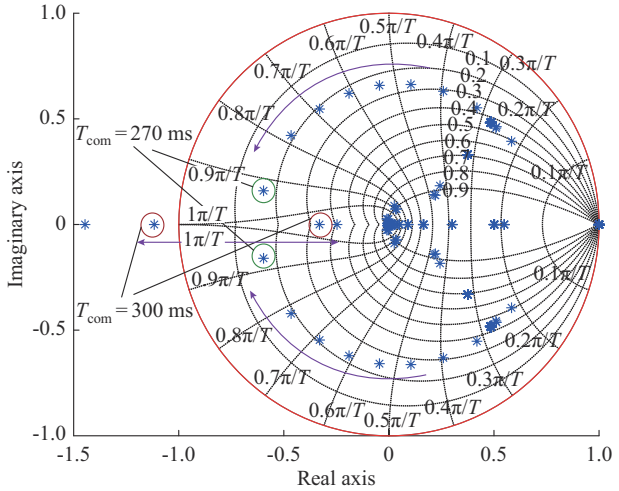

Fig. 7. Root contour with T_{com} changing from 30 to 300 ms with a step of 30 ms.

In the following, the upper bounds of tolerable communication rate T_{com} under different gains K_{psv} and K_{isv} are obtained using an exhaustive method. K_{psv} is set to be a value between 1 and 2 with a step of 0.05 and K_{isv} is set to be a value between 50 and 250 with a step of 25. Under each set of gains, the communication rate changes from 1 to 100 ms with a step of 1 ms. The largest communication rate that maintains the system stability is regarded as the upper bounds under the corresponding controller gains.

The tolerable communication rate of the proposed scheme under different K_{psv} and K_{isv} is compared with that of the DCA-based scheme in Fig. 8. As can be observed from Fig. 8, generally, when K_{psv} and K_{isv} become larger, the tolerable communication rate becomes lower. Compared with the DCA-based scheme, the proposed scheme guarantees the system stability at a lower communication rate.

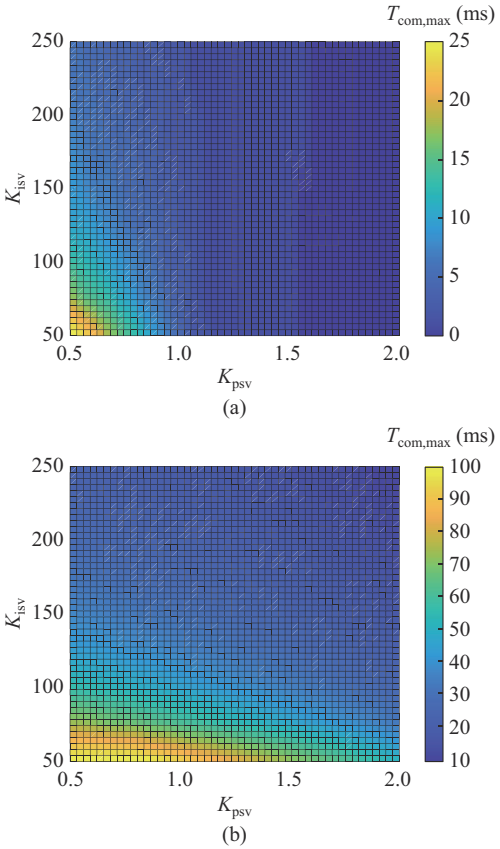

Fig. 8. Tolerable communication rate of proposed scheme and DCA-based scheme. (a) Proposed scheme. (b) DCA-based scheme.

V. Results and Discussions

The proposed scheme is tested through real-time simulations with 1-μs step size on OPAL-RT OP 5700 platform as depicted in Appendix A Fig. A1. The tested MG is shown in Fig. 2. Specifications of the MG are listed in Table III. Tie-line and load parameters are listed in Table IV.

A. Performance Evaluation

In this case, the performance of the proposed scheme is tested under load change to illustrate its effectiveness. The secondary control is activated at 0.5 s. The CPLs on bus 2 and bus 4 increase from 300 W to 600 W at 1.0 s. The resistive load on bus 1 changes from 13 Ω to 4.3 Ω at 1.0 s and back to 13 Ω at 1.8 s. The dynamic performance of the proposed scheme is compared with that of the DCA-based

scheme in [42] and the unified secondary control scheme in [44], as shown in Figs. 9 and 10.

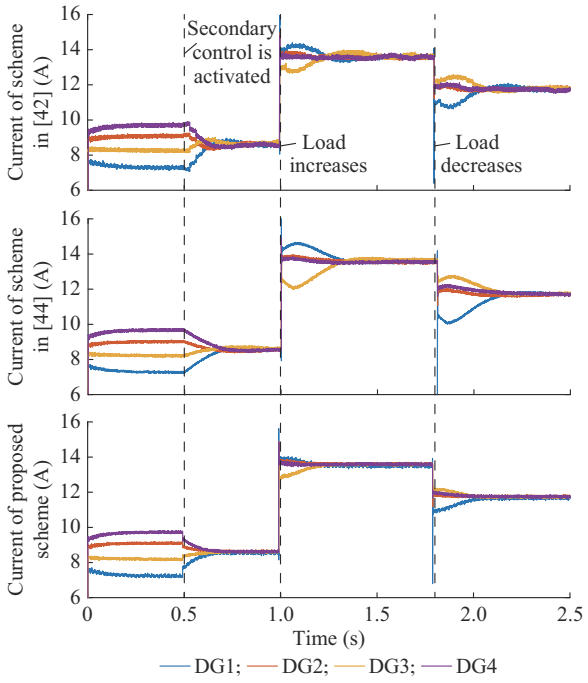

Fig. 9. Current sharing performance of different schemes.

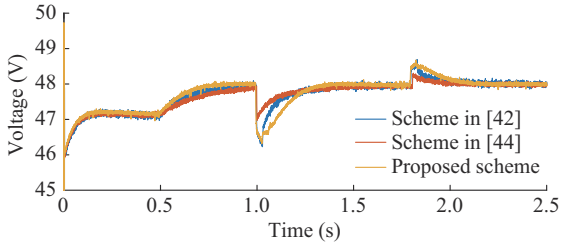

Fig. 10. Comparison of average voltage restoration performances.

After 0.5 s, under the proposed scheme, the output currents are accurately shared. When the load increases at 1.0 s and decreases at 1.7 s, accurate current sharing is still guaranteed by the secondary control. Also, as Fig. 11 shows, after secondary control is activated, the average bus voltage is regulated to the nominal value and is maintained regardless of load changes at 1.0 s and 1.8 s. The performance indexes such as the convergence time and overshoots are listed in Table V. Although the overshoot of the average voltage is larger, the proposed scheme has a faster convergence speed. The comparison with the schemes in [42] and [44] validates the advantage of the proposed scheme.

TABLE V
PERFORMANCE INDEXES OF SCHEMES IN [42], [44] AND PROPOSED SCHEME

Scheme	Convergence time for current sharing (s)	Convergence time for voltage regulation (s)	Overshoot of average voltage (V)
[42]	0.4	0.9	1.8
[44]	0.4	0.5	1.0
Proposed	0.2	0.3	1.8

Furthermore, the communication rate and convergence speed of the proposed scheme are also compared with those of the fixed-time/finite-time schemes, as shown in Table VI. It is shown that the proposed scheme reduces the convergence time in similar communication conditions.

TABLE VI
COMPARISON OF COMMUNICATION RATE AND CONVERGENCE SPEED OF PROPOSED SCHEME AND FIXED-TIME/FINITE-TIME SCHEMES

Scheme	Communication rate (ms)	Convergence time (s)
[22]	29	0.50
[23]	20	0.25
[24]	6	0.30
[25]	10	0.26
Proposed	10	0.20

B. Effect of Communication Rate

In practice, cooperative control schemes are usually faced with different intricacies in cyber systems, such as delay and data packet loss. Packet loss and other communication failures are often addressed by retransmission, which, as well as delay, decreases effective communication rate in essence. Therefore, system performance of the proposed scheme under different communication rates is also evaluated and shown in Fig. 11. Besides, system performance of different schemes with $T_{com}=100$ ms is shown in Fig. 12. The MG undergoes the same load changes as mentioned above.

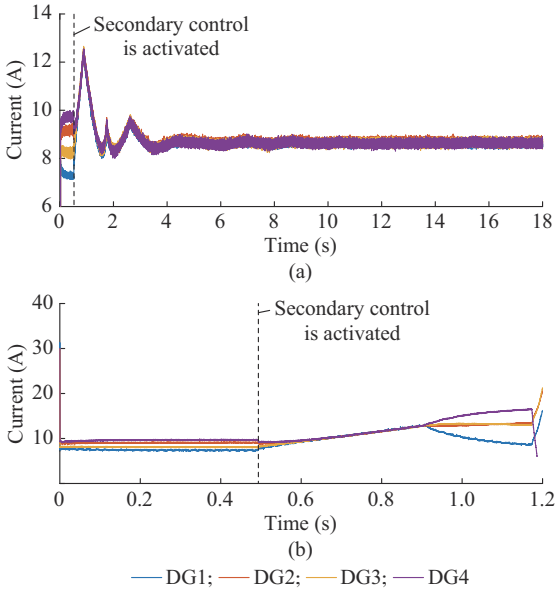

Fig. 11. Current sharing performance of proposed scheme under different communication rates. (a) $T_{com}=260$ ms. (b) $T_{com}=300$ ms.

It is shown in Fig. 11 that when T_{com} reaches 260 ms, the system is still stable, while a communication rate of 300 ms destabilizes the system, which is consistent with eigenvalue analysis as shown in Fig. 7.

It is observed in Fig. 12(a) that when T_{com}=100 ms, which indicates a lower communication rate, the settling time becomes longer. Nevertheless, desired current sharing and volt-

age restoration are still achieved. Correspondingly, the system is already unstable under the DCA-based scheme when T_{com} increases to 100 ms, as shown in Fig. 12(b).

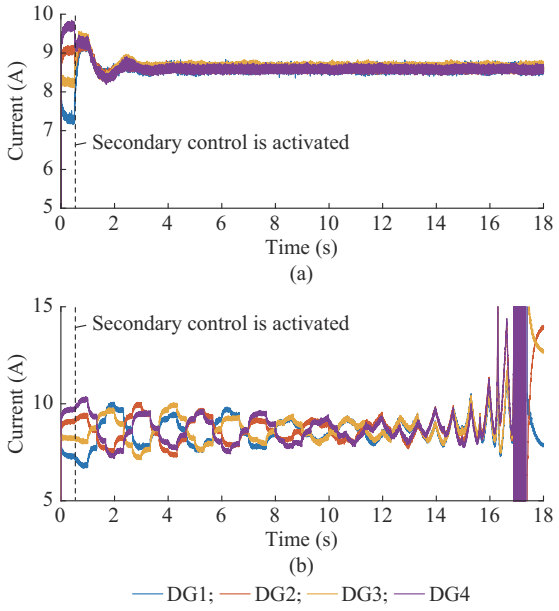

Fig. 12. Current sharing performance with $T_{com} = 100$ ms. (a) Proposed scheme. (b) DCA-based scheme.

C. Communication Link Failure

System resiliency to communication link failure is also studied. The secondary control is activated at 0.5 s. The CPLs on bus 2 and bus 4 increase from 300 W to 600 W at 0.8 s. The resistive load changes from 13 Ω to 4.3 Ω at 1.5 s and back to 13 Ω at 2.5 s. The communication link between converters 1 and 4 abruptly fails at 1.0 s and recovers at 2.6 s.

As shown in Fig. 13(a), before the failure at 0.6 s, it takes 0.2 s for currents to converge. Accurate current sharing is still achieved under the communication link failure and the load change afterwards. Although the broken link is recovered at 1.5 s in the middle of converging process, the system stability is guaranteed and currents can still converge within 0.3 s. Also, the average voltage is well maintained during the link failure as well as during the load changes, as shown in Fig. 13(b).

D. Converter Fault

In this case, system resiliency to a converter fault is studied. The secondary control is activated at 0.5 s. Converter 3 breaks down at 1.5 s and recovers at 2.5 s. A change in communication network comes along with the fault. As shown in Fig. 14(a), after converter 3 breaks down, the other 3 converters are still able to share the load current proportionately. After converter 3 recovers, its output current restores from 0 and reaches a consensus with the output currents of the other 3 converters. Besides, Fig. 14(b) shows that the average bus voltage of converters is well maintained at 48 V regardless of converter fault.

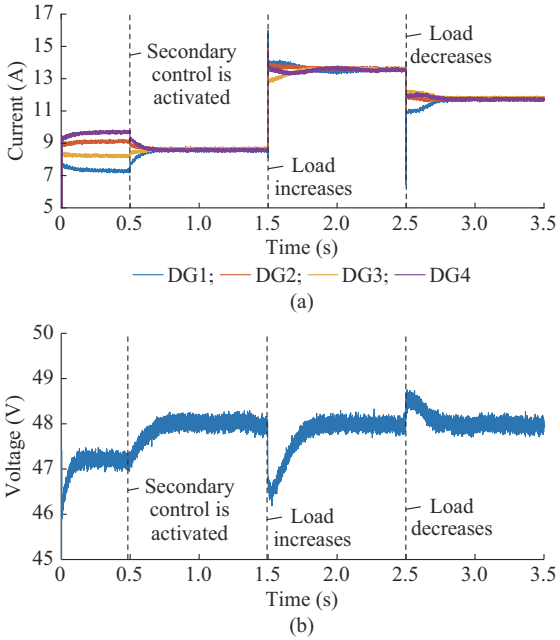

Fig. 13. System performance under communication link failure. (a) Current sharing. (b) Average voltage regulation.

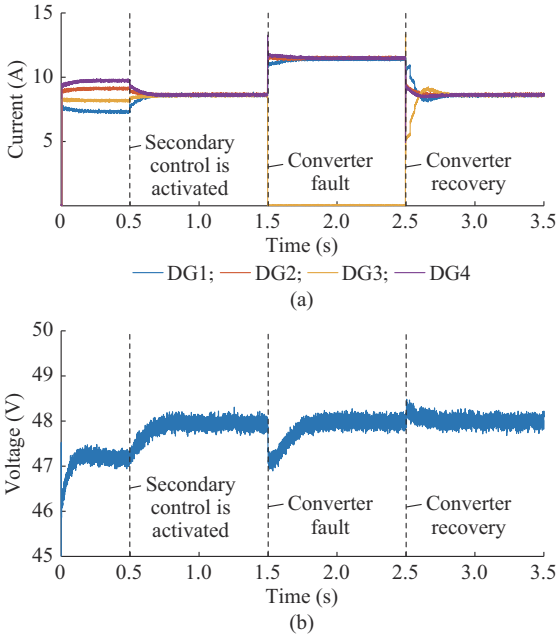

Fig. 14. System performance under converter fault. (a) Current sharing. (b) Average voltage regulation.

E. Discussion

As shown by the stability analysis and real-time simulation results, the proposed scheme reduces the convergence time and enhances the stability in the presence of high communication rates. However, when the number of converters increases, the communication process time also increases, leading to higher communication rates. Thus, the proposed scheme offers advantages in scenarios involving numerous converters.

However, the addition of a correction step to DDA, as presented in (3), increases its intermediate variables to $2n$. In

comparison, DCA and traditional diffusion algorithms contain only n intermediate variables. As the number of converters increases, the computational and memory requirements of the proposed scheme may also increase.

VI. Conclusion

This paper proposes a distributed secondary control scheme based on DDA to achieve average voltage restoration and proportional current sharing in DC MGs by sending a voltage shifting signal to the primary control. Main findings of this paper can be summarized as follows.

1) A dynamic variant of diffusion, DDA, is introduced and the proposed distributed secondary control scheme using DDA can achieve accurate current sharing among converters and bus voltage regulation in a distributed way. The proposed scheme is shown to have faster convergence speed than conventional control scheme utilizing consensus algorithm.

2) Based on an overall DT model of a DC MG, a specific range of communication and control parameters ensuring system stability is obtained according to root contours.

3) The tolerable communication rates under different control parameters are approximated using exhaustion method verifying that the MG using the proposed scheme is able to keep stable under a lower communication rate than the conventional DCA-based scheme.

Appendix A

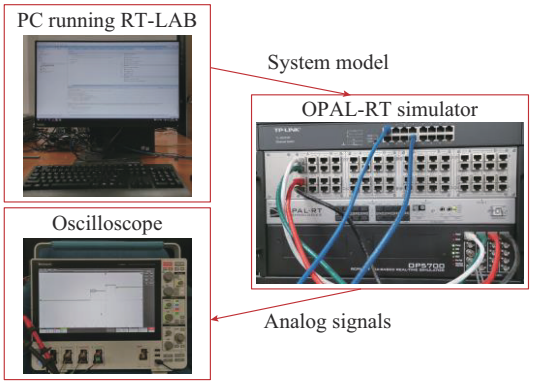

Fig. A1. Real-time simulation platform setup.

References

[1] T. Dragicevic, X. Lu, J. Vasquez *et al*., "DC microgrids – part I: a review of control strategies and stabilization techniques," *IEEE Transactions on Power Electronics*, vol. 31, no. 7, pp. 4876-4891, Jul. 2016.

[2] Z. Jin, L. Meng, J. M. Guerrero *et al*., "Hierarchical control design for a shipboard power system with DC distribution and energy storage aboard future more-electric ships," *IEEE Transactions on Industrial Informatics*, vol. 14, no. 2, pp. 703-714, Feb. 2018.

[3] F. Gao, S. Bozhko, A. Costabeber *et al*., "Control design and voltage stability analysis of a droop-controlled electrical power system for more electric aircraft," *IEEE Transactions on Industrial Electronics*, vol. 64, no. 12, pp. 9271-9281, Dec. 2017.

[4] A. Bidram and A. Davoudi, "Hierarchical structure of microgrids control system," *IEEE Transactions on Smart Grid*, vol. 3, no. 4, pp. 1963-1976, Dec. 2012.

[5] F. Gao, R. Kang, J. Cao *et al*., "Primary and secondary control in DC microgrids: a review," *Journal of Modern Power Systems and Clean Energy*, vol. 7, no. 2, pp. 227-242, Mar. 2019.

[6] J. M. Guerrero, M. Chandorkar, T.-L. Lee *et al*., "Advanced control architectures for intelligent microgrids – part I: decentralized and hierarchical control," *IEEE Transactions on Industrial Electronics*, vol. 60, no. 4, pp. 1254-1262, Apr. 2013.

[7] F. Gao, S. Bozhko, G. Asher *et al*., "An improved voltage compensation approach in a droop-controlled DC power system for the more electric aircraft," *IEEE Transactions on Power Electronics*, vol. 31, no. 10, pp. 7369-7383, Oct. 2016.

[8] V. Nasirian, Q. Shafiee, J. M. Guerrero *et al*., "Droop-free distributed control for AC microgrids," *IEEE Transactions on Power Electronics*, vol. 31, no. 2, pp. 1600-1617, Feb. 2016.

[9] Q. Shafiee, V. Nasirian, J. C. Vasquez *et al*., "A multi-functional fully distributed control framework for AC microgrids," *IEEE Transactions on Smart Grid*, vol. 9, no. 4, pp. 3247-3258, Jul. 2018.

[10] S. Peyghami, H. Mokhtari, P. C. Loh *et al*., "Distributed primary and secondary power sharing in a droop-controlled LVDC microgrid with merged AC and DC characteristics," *IEEE Transactions on Smart Grid*, vol. 9, no. 3, pp. 2284-2294, May 2018.

[11] T. R. Oliveira, W. W. A. G. Silva, and P. F. Donoso-Garcia, "Distributed secondary level control for energy storage management in DC microgrids," *IEEE Transactions on Smart Grid*, vol. 8, no. 6, pp. 2597-2607, Nov. 2017.

[12] P. Wang, X. Lu, X. Yang *et al*., "An improved distributed secondary control method for DC microgrids with enhanced dynamic current sharing performance," *IEEE Transactions on Power Electronics*, vol. 31, no. 9, pp. 6658-6673, Sept. 2016.

[13] P. C. Loh, F. Blaabjerg, S. Peyghami-Akhuleh *et al*., "Distributed secondary control in DC microgrids with low-bandwidth communication link," in *Proceedings of 2016 7th Power Electronics and Drive Systems Technologies Conference (PEDSTC)*, Tehran, Iran, Feb. 2016, pp. 641-645.

[14] G. Lou, W. Gu, X. Lu *et al*., "Distributed secondary voltage control in islanded microgrids with consideration of communication network and time delays," *IEEE Transactions on Smart Grid*, vol. 11, no. 5, pp. 3702-3715, Sept. 2020.

[15] M. Dong, L. Li, Y. Nie *et al*., "Stability analysis of a novel distributed secondary control considering communication delay in DC microgrids," *IEEE Transactions on Smart Grid*, vol. 10, no. 6, pp. 6690-6700, Nov. 2019.

[16] Z. Li, Z. Cheng, J. Si *et al*., "Distributed event-triggered secondary control for average bus voltage regulation and proportional load sharing of DC microgrid," *Journal of Modern Power Systems and Clean Energy*, vol. 10, no. 3, pp. 678-688, May 2022.

[17] M. Cucuzzella, S. Trip, C. de Persis *et al*., "A robust consensus algorithm for current sharing and voltage regulation in DC microgrids," *IEEE Transactions on Control System Technology*, vol. 27, no. 4, pp. 1583-1595, Jul. 2019.

[18] M. Cucuzzella, K. C. Kosaraju, and J. M. A. Scherpen, "Distributed passivity-based control of DC microgrids," in *Proceedings of 2019 American Control Conference (ACC)*, Philadelphia, USA, Jul. 2019, pp. 652-657.

[19] V. Nasirian, A. Davoudi, F. L. Lewis *et al*., "Distributed adaptive droop control for DC distribution systems," *IEEE Transactions on Energy Conversion*, vol. 29, no. 4, pp. 944-956, Dec. 2014.

[20] M. Shi, X. Chen, J. Zhou *et al*., "Distributed optimal control of energy storages in a DC microgrid with communication delay," *IEEE Transactions on Smart Grid*, vol. 11, no. 3, pp. 2033-2042, May 2020.

[21] Y. Du, H. Tu, H. Yu *et al*., "Accurate consensus-based distributed averaging with variable time delay in support of distributed secondary control algorithms," *IEEE Transactions on Smart Grid*, vol. 11, no. 4, pp. 2918-2928, Jul. 2020.

[22] S. Sahoo and S. Mishra, "A distributed finite-time secondary average voltage regulation and current sharing controller for DC microgrids," *IEEE Transactions on Smart Grid*, vol. 10, no. 1, pp. 282-292, Jan. 2019.

[23] Q. Yuan, Y. Wang, X. Liu *et al*., "Distributed fixed-time secondary control for DC microgrid via dynamic average consensus," *IEEE Transactions on Sustainable Energy*, vol. 12, no. 4, pp. 2008-2018, Oct. 2021.

[24] S. Sahoo, S. Mishra, S. M. Fazeli *et al*., "A distributed fixed-time secondary controller for DC microgrid clusters," *IEEE Transactions on Energy Conversion*, vol. 34, no. 4, pp. 1997-2007, Dec. 2019.

[25] P. Wang, R. Huang, M. Zaery *et al*., "A fully distributed fixed-time secondary controller for DC microgrids," *IEEE Transactions on Industrial Application*, vol. 56, no. 6, pp. 6586-6597, Nov.-Dec. 2020.

[26] S.-Y. Tu and A. H. Sayed, "Diffusion strategies outperform consensus strategies for distributed estimation over adaptive networks," *IEEE*

Transactions on Signal Processing, vol. 60, no. 12, pp. 6217-6234, Dec. 2012.
[27] H. J. Yoo, T. T. Nguyen, and H. M. Kim, "Diffusion-based distributed coordination control of power converters in MG for efficiency improvement," *IEEE Access*, vol. 7, pp. 53347-53357, Apr. 2019.
[28] R. de Azevedo, M. H. Cintuglu, T. Ma *et al*., "Multiagent-based optimal microgrid control using fully distributed diffusion strategy," *IEEE Transactions on Smart Grid*, vol. 8, no. 4, pp. 1997-2008, Jul. 2017.
[29] V. H. Bui, A. Hussain, and H. M. Kim, "Diffusion strategy-based distributed operation of microgrids using multiagent system," *Energies*, vol. 10, no. 7, pp. 1-21, Jul. 2017.
[30] Y. He, W. Wang, and X. Wu, "Multi-agent based fully distributed economic dispatch in microgrid using exact diffusion strategy," *IEEE Access*, vol. 8, pp. 7020-7031, Dec. 2020.
[31] T. T. Nguyen and H. M. Kim, "Leader-following diffusion-based reactive power coordination and voltage control of offshore wind farm," *IEEE Access*, vol. 8, pp. 149555-149568, Aug. 2020.
[32] J. Yu, F. Gao, S. Wei *et al*., "An improved distributed secondary control scheme in islanded AC microgrids," in *Proceedings of 2020 IEEE Energy Conversion Congress and Exposition (ECCE)*, Detroit, USA, Oct. 2020, pp. 1335-1342.
[33] D. Liao, F. Gao, Y. Zhao *et al*., "A dynamic diffusion algorithm for distributed secondary control of DC microgrids," in *Proceedings of 2020 IEEE Energy Conversion Congress and Exposition (ECCE)*, Detroit, USA, Oct. 2020, pp. 1299-1306.
[34] B. Fan, J. Peng, Q. Yang *et al*., "Distributed periodic event-triggered algorithm for current sharing and voltage regulation in DC microgrids," *IEEE Transactions on Smart Grid*, vol. 11, no. 1, pp. 577-589, Jan. 2020.
[35] J. Peng, B. Fan, Q. Yang *et al*., "Fully distributed discrete-time control of DC microgrids with ZIP loads," *IEEE System Journal*, vol. 16, no. 1, pp. 155-165, Mar. 2022.
[36] L. Xing, Y. Qi, X. Liu *et al*., "Discrete-time distributed secondary control for DC microgrids via virtual voltage drop averaging," *IEEE Transactions on Sustainable Energy*, vol. 14, no. 1, pp. 272-282, Jan. 2023.
[37] L. Xing, F. Guo, X. Liu *et al*., "Voltage restoration and adjustable current sharing for DC microgrid with time delay via distributed secondary control," *IEEE Transactions on Sustainable Energy*, vol. 12, no. 2, pp. 1068-1077, Apr. 2021.
[38] A. H. Sayed, "Diffusion adaptation over networks," in *Academic Press Library in Signal Processing*. Amsterdam: Elsevier, 2014, pp. 323-453.
[39] J. Chen and A. H. Sayed, "Diffusion adaptation strategies for distributed optimization and learning over networks," *IEEE Transactions on Signal Processing*, vol. 60, no. 8, pp. 4289-4305, Aug. 2012.
[40] K. Yuan, B. Ying, X. Zhao *et al*., "Exact diffusion for distributed optimization and learning – part I: algorithm development," *IEEE Transactions on Signal Processing*, vol. 67, no. 3, pp. 708-723, Feb. 2019.
[41] B. Ying, K. Yuan, and A. H. Sayed, "Dynamic average diffusion with randomized coordinate updates," *IEEE Transactions on Signal and Information Processing Over Networks*, vol. 5, no. 4, pp. 753-767, Dec. 2019.
[42] L. Meng, T. Dragicevic, J. Roldan-Perez *et al*., "Modeling and sensitivity study of consensus algorithm-based distributed hierarchical control for DC microgrids," *IEEE Transactions on Smart Grid*, vol. 7, no. 3, pp. 1504-1515, May 2016.
[43] X. Lu, J. M. Guerrero, K. Sun *et al*., "An improved droop control method for DC microgrids based on low bandwidth communication with DC bus voltage restoration and enhanced current sharing accuracy," *IEEE Transactions on Power Electronics*, vol. 29, no. 4, pp. 1800-1812, Apr. 2014.
[44] Q. Zhang, Y. Zeng, Y. Liu *et al.*, "An improved distributed cooperative control strategy for multiple energy storages parallel in islanded DC microgrid," *IEEE Journal of Emerging and Selected Topics in Power Electronics*, vol. 10, no. 1, pp. 455-468, Feb. 2022.

Dawei Liao received the B.E. degree in electrical engineering and the M.S. degree in electrical engineering from Shanghai Jiao Tong University, Shanghai, China, in 2020 and 2023, respectively. His research interests include distributed control, modeling and stability of microgrids.

Fei Gao received the Ph.D. degree in electrical engineering from the Power Electronics, Machines, and Control Research Group, University of Nottingham, Nottingham, U.K., in 2016. From 2016 to 2019, he was a Postdoctoral Researcher with the Department of Engineering Science, University of Oxford, Oxford, U.K.. Since July 2019, he has been an Associate Professor with Shanghai Jiao Tong University, Shanghai, China. His research interests include modeling, control, power management and stability of microgrids, and more-electric transportation systems.

Daniel J. Rogers received the M.Eng. and Ph.D. degrees in electrical and electronic engineering from Imperial College London, London, U.K., in 2007 and 2011, respectively. He is an Associate Professor with the Department of Engineering Science, University of Oxford, Oxford, U.K.. His research interests include the use of medium- and large-scale power electronic systems to create flexible electrical networks that take advantage of a diverse range of generation and storage technologies.

Wentao Huang received the Ph.D. degree in electrical engineering from Shanghai Jiao Tong University, Shanghai, China, in 2015. He is currently an Associate Professor with the Department of Power Electrical Engineering, Shanghai Jiao Tong University. His research interests include protection and control of active distribution systems, microgrids, smart grid, and renewable energy.

Dong Liu received the B.S. and M.S. degrees from Sichuan University, Chengdu, China, in 1989 and 1994, respectively, and the Ph.D. degree from Southeast University, Nanjing, China, in 1997. He is currently a Full Professor with Electrical Engineering Department, Shanghai Jiao Tong University, Shanghai, China. His research interests include smart grids and cyber-physical systems for power grids.

Houjun Tang received the Ph.D. degree in automation from Yamagata University, Yamagata, Japan, in 1997. He is currently a Full Professor with the Department of Electrical Engineering, Shanghai Jiao Tong University, Shanghai, China. His research interests include wireless power transform, motor drive inverters, and power converters.